Operation of Offshore Wind Farms Connected with DRU-HVDC Transmission Systems with Special Consideration of Faults

R. LI, L. YU, and L. XU

Department of Electronic and Electrical Engineering, University of Strathclyde, Glasgow, G1 1XW, UK
Corresponding Author: L. XU, E-mail: lie.xu@strath.ac.uk
Other Authors' E-mail: rui.li@strath.ac.uk, lujie.yu@strath.ac.uk

Abstract The diode rectifier unit (DRU)-based high-voltage DC (DRU-HVDC) system is a promising solution for offshore wind energy transmission thanks to its compact design, high efficiency, and strong reliability. Herein we investigate the feasibility of the DRU-HVDC system considering onshore and offshore AC grid faults, DC cable faults, and internal DRU faults. To ensure safe operation during the faults, the wind turbine (WT) converters are designed to operate in either current-limiting or voltage-limiting mode to limit potential excessive overcurrent or overvoltage. Strategies for providing fault currents using WT converters during offshore AC faults to enable offshore overcurrent and differential fault protection are investigated. The DRU-HVDC system is robust against various faults, and it can automatically restore power transmission after fault isolation. Simulation results confirm the system performance under various fault conditions.

Keywords: Diode rectifier unit (DRU), fault protection, HVDC transmission, offshore wind farm.

1 Introduction

With the advancement of high-voltage DC (HVDC) technology based on voltage source converters (VSCs), there have been significant developments in HVDC-connected offshore wind farms (OWFs) [1, 2]. To reduce the cost related to offshore wind power integration, diode rectifier unit (DRU)-based HVDC systems have recently received notable interest [3-9]. By replacing the VSC of an offshore station with a diode rectifier, in addition to the significant reduction of volume and weight, transmission losses and total cost can be potentially reduced by up to 20% and 30%, respectively, and the transmission capacity can be increased by 33% [4, 10]. DRU-HVDC systems also have the advantages of high reliability, modular design, full encapsulation, and reduced operation and maintenance costs [4, 10, 11].

Since the DRU is effectively a passive device with no controllability, the OWF AC system must be regulated and controlled by the wind turbines (WTs). Voltage and frequency control of an offshore network by WTs connected to a DRU-HVDC system was proposed in [3], which proves that such a solution is technically feasible in steady states and during various transients. The developed control scheme was further tested and validated during three-phase faults at the onshore HVDC converter AC terminals [7]. However, the proposed control requires measurements at the point of common connection (PCC) for each WT, necessitating the need for high-speed communication.

Various fault cases, including DC faults and symmetrical onshore and offshore AC faults were investigated in [8]. However, during an offshore AC fault, the AC currents of the WT converters were simply controlled at zero without considering the need for the operation of the protection relays. An energy management scheme was introduced in [9] to regulate the input and output power of the DRU-HVDC links, and its low voltage ride-through (LVRT) capability was further verified. However, the WTs were modeled as ideal voltage sources, and the interactions between the WTs and DRU stations were ignored.

In [12], the *dq* reference frame was directly obtained by integrating the desired frequency (e.g. 50 Hz); thus, the offshore frequency was fixed at 50 Hz during an offshore AC fault. However, in the study, the OWFs were simplified as controllable current sources, and the dynamics of the WT converters were omitted. A

distributed phase-locked loop (PLL)-based control was proposed in [13] to share reactive power among WTs without communication. With the developed controller, the system could ride through onshore and offshore AC faults.

Fast fault current injection control was proposed in [14] to regulate the WT currents during fault transients and enable overcurrent and differential protection. The negative-sequence current controller was also developed to ride through asymmetrical offshore AC faults. However, DC cable faults and DRU internal faults were not addressed.

Herein we investigate the operation of a DRU-HVDC system considering WT control and operation requirements during faults including onshore and offshore AC grid faults, DC cable faults, and internal DRU faults. The paper is organized as follows. Section 2 describes the layout of the offshore wind power system with a DRU-HVDC system. Section 3 presents a generalized WT control strategy. Section 4 discusses the specific behaviors of the WT control during various faults and the actions of protection relays. Section 5 presents simulation studies on the DRU-HVDC during various faults. Finally, Section 6 draws the conclusions.

2 System Structure

The layout of a 1200-MW offshore wind power transmission system with DRU-HVDCs is illustrated in **Fig. 1**. The wind farm consists of three WT clusters, wherein each cluster has six strings containing a total of fifty 8-MW WTs. Strings 1 and 2 each contain nine WTs, whereas the other strings each have eight WTs.

As shown in **Fig. 1**, three DRUs are connected in series on the DC side to boost the DC voltage, whereas the AC sides are connected in parallel to the wind farm clusters. Each DRU comprises two series-connected 12-pulse bridges with star-star-delta three-winding transformers on the AC side. Filters are connected on the AC side of each DRU for reactive power compensation and harmonic suppression. The full-bridge (FB) submodule (SM)-based modular multilevel converter (MMC) is adopted for the onshore station [15], which regulates the DC voltage.

3 General Control Strategy

When connected to a DRU-HVDC system, the WT front-end converters (FECs) have to form the offshore AC system with controlled AC voltage magnitude and frequency, and transmit active power generated by the WTs [15]. The WT controls represented in this section specifically include the fault response functions. The fundamental operation, which has been studied previously, is also being tested as part of pre-fault and post-fault operations. **Fig. 2** shows the overall structure of the system control for the WT FECs [15]. The detailed functions and designs of the individual control block are described in this section.

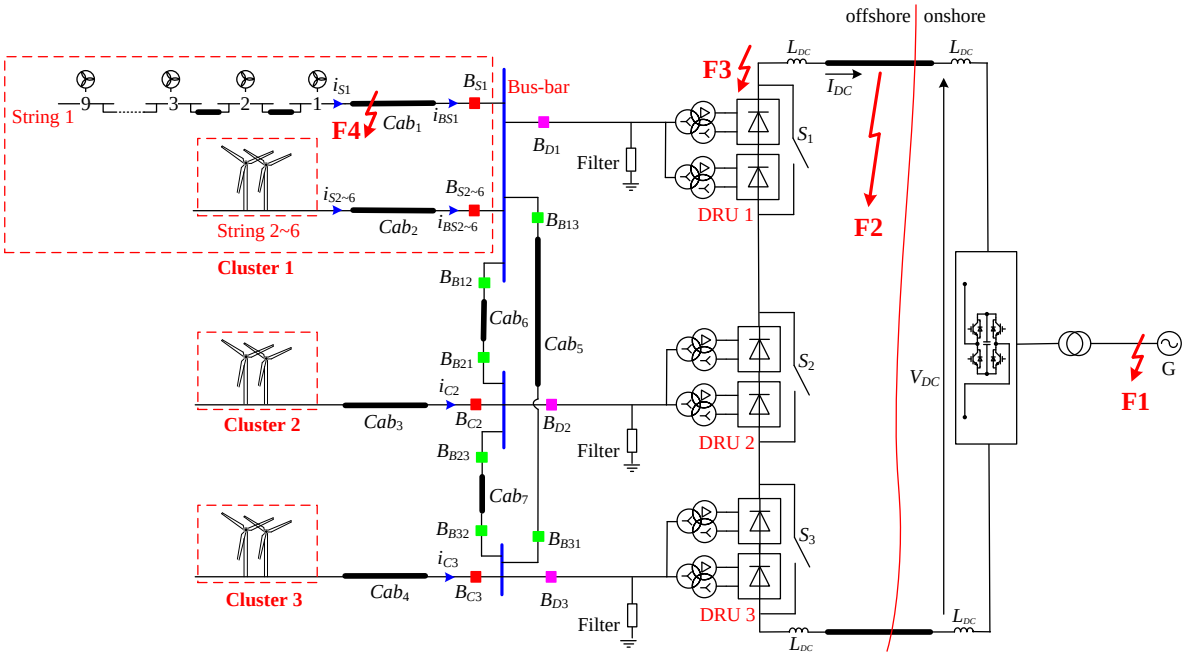

Fig. 1 System layout of offshore wind farms connected to a DRU-HVDC system.

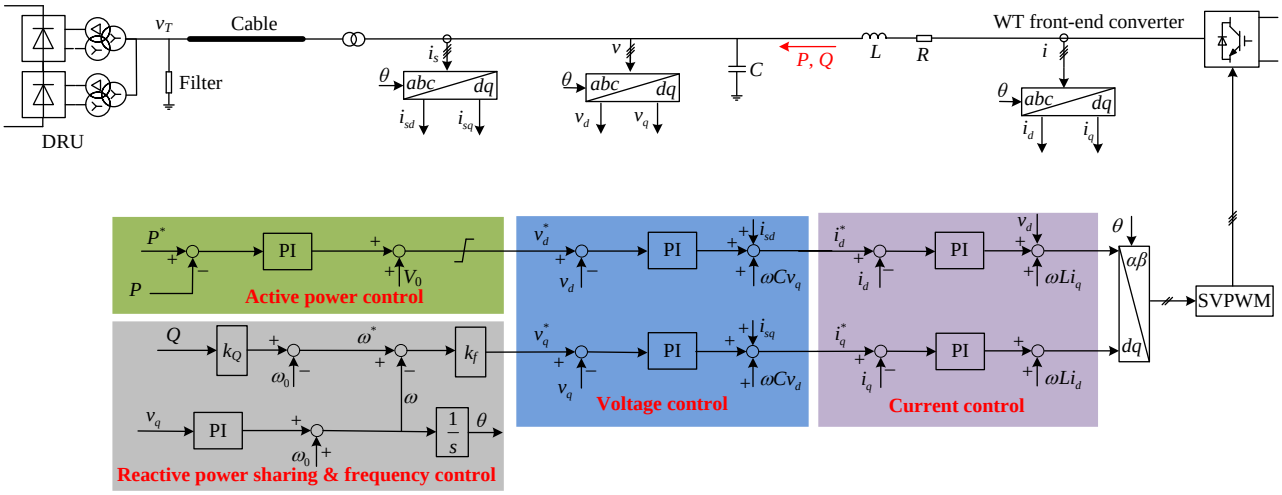

Fig. 2 Control structure of wind turbine front-end converters connected to a DRU-HVDC system.

1) Current control loop

To improve the dynamics of the system and limit fault currents during faults, an inner current control loop is adopted. During faults, the upper control loops may saturate and set the reference currents, i_d^* and i_q^*, to their maximum values to avoid overcurrents. The fault currents provided by the WT converters also enable offshore overcurrent and differential fault protection.

2) Offshore AC voltage control loop

The offshore network is built up by WT converters and the AC voltage controller is implemented to regulate the offshore AC voltage. During onshore AC grid faults, which may severely limit the active power transmitted from the OWF to the onshore AC grid, the DC voltage of the DRU-HVDC system could increase. The AC voltage control loop is used to effectively limit the DC and offshore AC voltages. During offshore AC faults, the offshore AC voltage drops and the AC voltage controller saturates and sets the reference currents to their maximum values.

3) Active power control loop

Because the WT generator-side converter controls the DC-link voltage, the active power control—i.e., the maximum power point tracking (MPPT) function—is performed by the FEC. Because the onshore MMC station controls its DC terminal voltage at the rated value, the active power generated by the wind farm can be controlled by adjusting the offshore AC voltage amplitude. As shown in **Fig. 2**, the active power control loop sets the reference voltage of the *d*-axis, v_d, to regulate the offshore AC voltage amplitude according to power generation. During severe faults that prevent the transmission of generated power from the WTs, e.g., onshore AC faults, the active power control loop saturates and sets the *d*-axis reference voltage, v_d^*, to its maximum value (1.1 pu in this paper).

4) Reactive power sharing and frequency control

During active power transmission, the DRU station also consumes reactive power, which needs to be compensated for by the AC-side filters and WT converters. Thus, the required reactive power needs to be equally shared among the individual WT converters. As illustrated in **Fig. 2**, the PLL is used to capture the offshore frequency, ω, while the reactive power and frequency droop (*Q-f*) regulates the reference frequency, ω^*. Such a control scheme ensures zero error between ω and ω^* as well as reactive power sharing as detailed in [13].

4 Control and Operation Consideration During Various Faults

The specific considerations to ensure satisfactory system operation are described in this section together with the actions of the protection relays under different faults.

4.1 Onshore AC faults

During an onshore AC fault (F1, **Fig. 1**), the onshore MMC can still fully control the AC current, but the power transmission capability of the MMC could decrease owing to the decrease of the AC grid voltage. If the imported energy from the OWF to the HVDC link through the DRUs is greater than the maximum power that can be exported by the onshore MMC, the DC voltage of the HVDC link and the MMC submodule capacitors will be charged by the power surplus leading to DC overvoltage.

With the increase of the DC voltage, the WT active power control loop saturates and the offshore voltage is set to its maximum value, e.g., 1.1 pu in this paper. The DRU station becomes reverse blocked and the power transmission drops to zero when the DC voltage exceeds the following threshold:

$$V_{th} = 12n\left(1.35V_{off\_\max} - \frac{3}{\pi}X_{AC}I_{DC}\right) \quad (1)$$

where $V_{off\_\max}$ is the maximum phase voltage of the offshore AC network (e.g., approximately 1.1 pu of the rated value), X_{AC} is the impedance of the DRU interface transformers, and n is the transformer ratio. After fault isolation, the onshore grid voltage restores and the DC voltage of the DRU-HVDC link and offshore power transmission gradually resumes normal operation without need for communication.

4.2 DC cable faults

Pole-to-pole DC faults are more serious than pole-to-ground faults considering the significant reduction of the HVDC link voltage and potential high DC fault current. However, pole-to-ground faults are more likely in cable schemes, so they are still considered in this section.

1) Pole-to-pole DC cable faults

After a solid pole-to-pole DC fault (F2, **Fig. 1**), the DC voltage of the DRU-HVDC link collapses. Owing to the negative-voltage generating capability of the FB submodules, the onshore MMC remains operational and continues to provide reactive power to support the onshore AC grid. The submodule capacitor voltages are fully controlled at the rated values; thus, fast restart after fault isolation can be realized.

The DC voltage collapse of the DRU-HVDC link also leads to a voltage drop in the offshore AC grid; thus, both the active power and voltage control loops of the WTs saturate. As the active power transmission is interrupted, the converters reduce the *d*-axis currents and increase the *q*-axis currents to their maximum values, providing fault currents, which enable fault detection. After several-hundred milliseconds, the WT converters may be blocked, as pole-to-pole DC cable faults are usually permanent and require the complete shutdown of the DC system (unless overhead DC lines are used, but they are not considered in this study).

2) Pole-to-ground DC cable faults

After a solid pole-to-ground fault (also F2, **Fig. 1**), the DC voltage of the faulty pole drops to approximately zero. As the FB SMs can generate negative voltages, the onshore FB-MMC station is still capable of controlling the DC voltage of the healthy pole to nearly match the rated value. Thus, the DRU-HVDC link operates at half of the rated DC voltage to continuously transmit power. However, as the DC voltage of the DRU-HVDC link is halved, the power transmission capability of the system is reduced under such asymmetrical DC faults.

The reduced DC voltage of the DRU-HVDC link also results in a drop of the offshore AC voltage, which leads to the saturation of the power and voltage control loops of the WTs. The WT FECs automatically operate in current-limiting mode to transmit part of the generated power to the system.

4.3 DRU station internal faults

After the internal fault of a DRU is detected (F3, **Fig. 1**), the DRUs need to be reconfigured. The faulty DRU needs to be isolated from the offshore AC network by opening the corresponding AC circuit breaker to prevent the fault from propagating to the offshore AC grid. On the DC side, the DC switch is closed to bypass the faulty DRU and provide a conduction path for the DC currents. The onshore FB-MMC actively reduces the DC voltage of the DRU-HVDC to approximately two thirds of the rated value to continuously transfer wind power using the other two healthy DRUs. Rather than shutting down the entire HVDC system, only the faulty DRU is bypassed while the healthy DRUs can continuously transfer power with reduced capability, thus maximizing system availability.

4.4 Offshore AC faults

After a fault on the offshore AC grid (F4, **Fig. 1**), the offshore grid voltage collapses, and both the power and voltage control loops saturate (similar to a pole-to-pole DC cable fault, as described in Subsection 4.2). Again, the *d*-axis currents are reduced while the *q*-axis currents of the WT FECs are increased to their maximum values, providing fault currents, which enable fault detection. After the faulty branch of the offshore network is isolated by AC circuit breakers, the offshore AC network recovers and power transmission can resume. Apart from a temporary loss of power transmission during the offshore AC fault, and potential permanent reduction of power generation from the wind farm due to the disconnection of the faulty branches, the operation of the onshore MMC is unaffected.

5 Case Study

The performance of the system shown in **Fig. 1** is assessed using PSCAD simulations, for which the system parameters are listed in **Table I**. To test the system performance during an offshore AC fault at a WT string, the fault string (String 1, **Fig. 1**) is represented by detailed converter models (Converters 1–9) while the other healthy strings in Cluster 1 (i.e., Strings 2–6) and Clusters 2 and 3 are modeled as lumped converters rated at 328 MW, 400 MW, and 400 MW (Converters 10, 11, and 12), respectively. In the simulation, the aggregated FECs and the DRU station are represented by detailed switching models while the onshore MMC station is represented by a detailed submodule-based switching function model [16].

Table I
PARAMETERS OF THE TESTED DRU-HVDC SYSTEM

Components	Parameters	Values
DRU-HVDC	Power	1200 MW
	DC voltage	±320 kV
12-pulse DRU	Transformer (Y/Y/Δ)	66/43.4/43.4 kV,
	Leakage inductance	0.18 pu
	Reactive power compensation	0.4 pu
Onshore MMC	Submodule capacitance	9200 μF
	Submodule number per arm N	256
	Submodule capacitor voltage	2.5 kV
	Arm inductance	0.1 pu
	Transformer (Y/Δ)	400/330 kV
WT converters	Power rating of individual WT	8 MW
	Transformer (Y/Δ)	3/66 kV
	Leakage inductance	0.1 pu
	Filter capacitor C	0.05 pu
	Converter reactance L	0.1 pu
	Switching frequency	2 kHz

5.1 Onshore AC faults

In this study, a solid symmetrical AC fault, F1 in **Fig. 1**, is applied at the transformer grid-side at t=0.5 s and cleared at t=0.64 s. The simulation results for the onshore and offshore systems are shown in **Fig. 3** and **Fig. 4**, respectively.

Once the fault occurs, the onshore AC voltage rapidly decreases to 0, as shown in **Fig. 3**(a). Consequently, the active power transmitted by the onshore MMC quickly decreases to 0, as shown in **Fig. 3**(e), yet the WT and DRU station still transmit the generated active power, as shown in **Fig. 4**(c). During the fault, the active current of the onshore MMC is reduced using a voltage-dependent current-order limit (VDCOL) while its reactive current is increased [17]. The unbalanced active power in the HVDC system leads to an increase in the DC voltage of the HVDC link from 1.0 pu to 1.38 pu in 0.08 s, as shown in **Fig. 3**(c). The increase of the DC voltage reduces the power transmitted to DC by the offshore DRU and that from the WTs, as shown in **Fig. 4**(c). When the DC voltage reaches 1.38 pu, the offshore AC voltage reaches the WT converter limit (set at 1.1 pu), as shown in **Fig. 4**(a); thus, no active power can be generated and transmitted to DC. The excess power in each individual WT needs to be dealt with as part of WT fault ride-through strategy, e.g., using DC damping resistors in the WTs, but these are not part of this study.

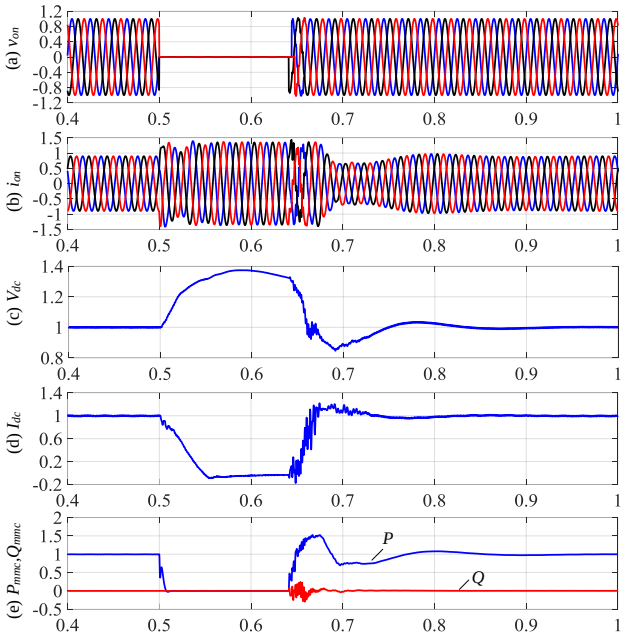

Fig. 3 Simulation results of onshore MMC during symmetrical onshore AC fault in per-unit terms: (a) three-phase AC voltages, (b) three-phase AC currents, (c) DC voltage, (d) DC current, and (e) active and reactive powers.

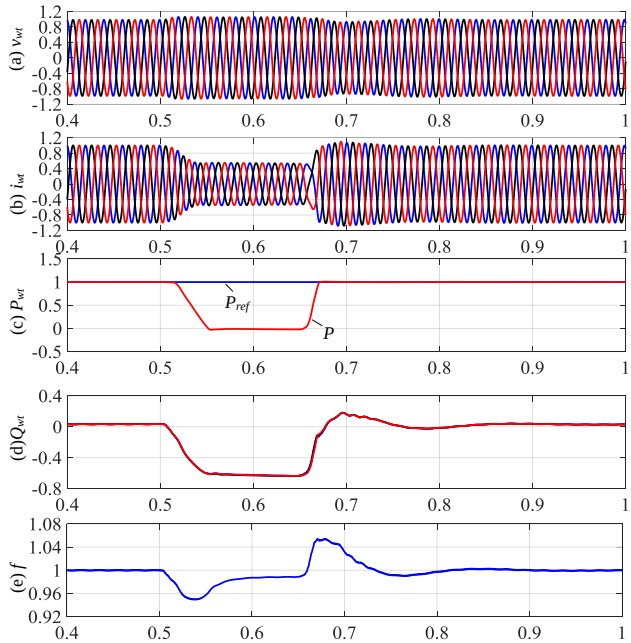

Fig. 4 Simulation results of WT converter during symmetrical onshore grid fault in per-unit terms: (a) three-phase AC voltages, (b) three-phase currents, (c) active power, (d) reactive power, and (e) frequency.

After fault initiation, the reactive power and *q*-axis current increase while the *d*-axis current decreases to avoid overcurrent. In addition, the reactive powers are shared among WT converters and the offshore frequency is well controlled near the rated value of 50 Hz, as shown in **Fig. 4**(d) and (e), respectively.

At 0.64 s, the fault is cleared and the onshore AC voltage recovers, leading to the increase of transmitted onshore active power, as shown in **Fig. 3**(e). **Fig. 4**(c) shows that wind power generation is also quickly restored.

The HVDC link experiences overvoltage (1.38 pu) during the solid symmetrical onshore fault. A DC chopper could be used to reduce such DC overvoltage if necessary. The DC overvoltage could also be reduced if the maximum AC voltage limit (set to 1.1 pu in this study) were reduced, which could be part of overall system design and optimization.

5.2 DC cable faults

The system performance during DC cable faults is assessed in this section, considering both DC pole-to-pole and pole-to-ground faults.

1) Pole-to-pole DC cable faults

A permanent solid pole-to-pole fault, F2 in **Fig. 1**, is applied at the middle of the DC cable at t=0.5 s. Under such a fault, it is impossible to transmit power to the onshore grid through the DRU-HVDC link, so the WT converters are shut-down 100 ms after fault initiation, while the onshore MMC station operates in STATCOM mode to support the onshore grid by providing reactive power.

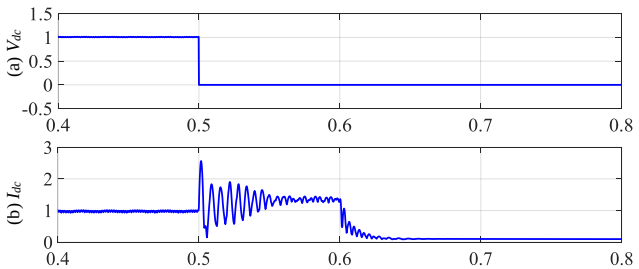

Fig. 5 Simulation results of DRU station during pole-to-pole DC cable fault in per-unit terms: (a) DC voltage and (b) DC current.

The DC voltage drops to zero after the DC fault, as shown in **Fig. 5**(a). This also causes a significant drop in the offshore AC voltage, as shown in **Fig. 6**(a). The WT FECs automatically operate in current-limiting mode to provide fault currents, which flow through the offshore grid and the DRU station to feed into the DC fault, as shown in **Fig. 5**(b) and **Fig. 6**(b), respectively. This contributes to the establishment of the offshore AC voltage to approximately 0.4 pu, as shown in **Fig. 6**(a), even though the system suffers a solid pole-to-pole DC fault. Oscillations are observed in the DC current of the DRU-HVDC during fault transients owing to the passive *R*, *L*, and *C* components in the offshore AC and DC systems, as shown in **Fig. 5**(b). The active power of the WTs drops to zero while the reactive power increases to approximately 0.5 pu to try to restore the offshore grid voltages, as shown in **Fig. 6**(c) and (d), respectively. As displayed in **Fig. 6**(e), the offshore frequency is well controlled near 50 Hz until the WT converters are blocked at t=0.6 s.

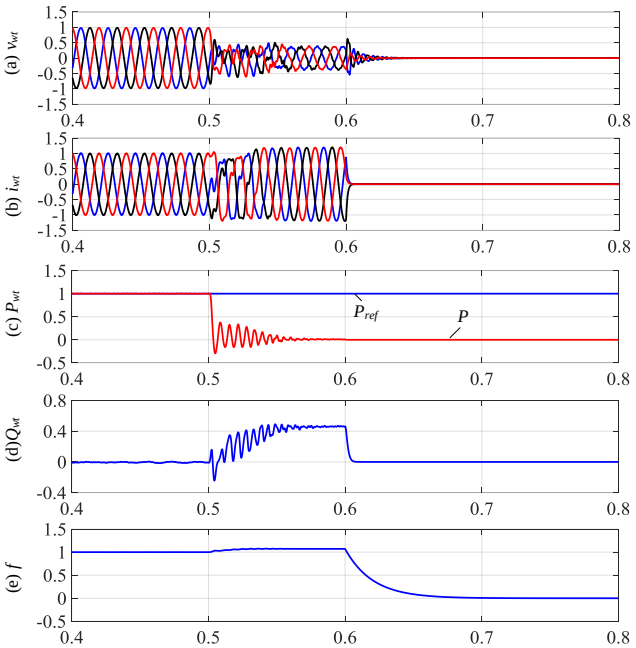

Fig. 6 Simulation results of offshore WT converter during pole-to-pole DC cable fault in per-unit terms: (a) three-phase AC voltages, (b) three-phase currents, (c) active power, (d) reactive power, and (e) frequency.

The results in **Fig. 7**(a) and (b) show that the DC side of the onshore MMC has behaviors similar to the offshore station during the DC fault. The onshore FB-MMC controls its terminal DC voltage and DC current around zero, and operates in STATCOM mode by continuously providing reactive power to the grid, as shown in **Fig. 7**(d). One hundred milliseconds after fault initiation (at t=0.6 s), the WT converters are blocked and the offshore AC network is de-energized considering the DC fault is permanent.

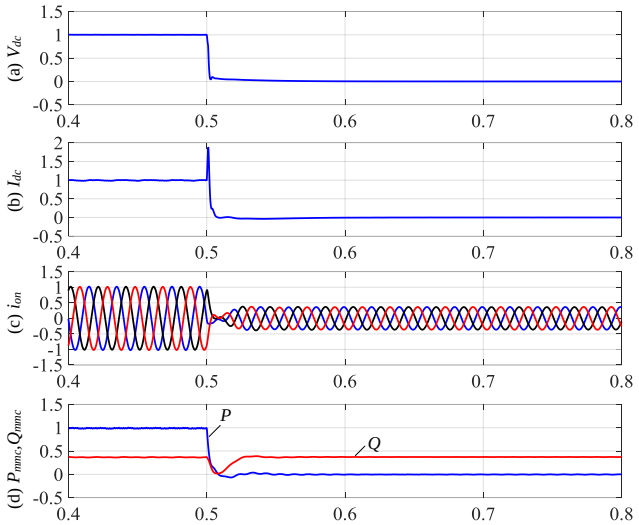

Fig. 7 Simulation results of onshore MMC during pole-to-pole DC cable fault in per-unit terms: (a) DC voltage, (b) DC current, (c) three-phase currents, and (d) active and reactive powers.

2) Pole-to-ground DC cable faults

A permanent solid pole-to-ground DC fault, F2 in **Fig. 1**, is applied at the positive pole at t=0.5 s, and the simulation results are shown in **Fig. 8** and **Fig. 9**.

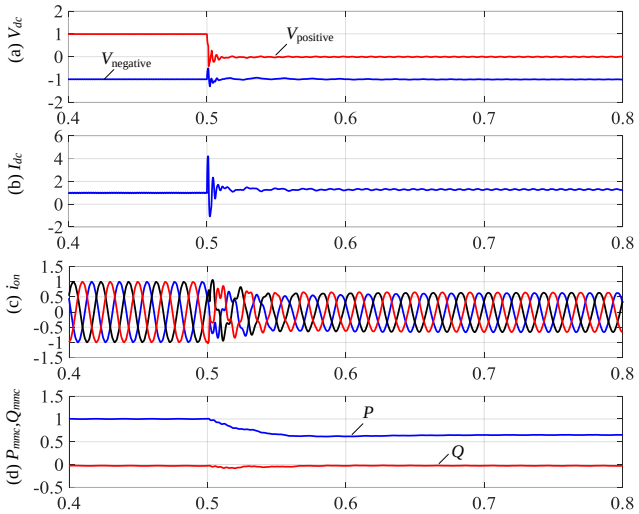

Fig. 8 Simulation results of onshore MMC during positive pole-to-ground DC cable fault in per-unit terms: (a) DC voltage, (b) DC current, (c) three-phase AC currents, and (d) active and reactive powers.

After fault initiation, the positive-pole DC voltage drops to zero, and for the adopted symmetrical monopole configuration, the onshore FB-MMC station continues to control the healthy negative-pole DC voltage near the rated value during such a pole-to-ground DC fault [18], as shown in **Fig. 8**(a). Therefore, the DRU-HVDC link operates at half of the rated DC voltage. With the reduced DC voltage, the DC current is increased to 1.25 pu (considering 25% overcurrent capability), and the onshore MMC AC current and the transmitted active power are reduced to 0.625 pu, as shown in **Fig. 8** (b), (c), and (d), respectively.

Owing to the reduced DRU-HVDC link voltage, the output voltage of the WT converters decreases to 0.65 pu, so the voltage control loop saturates and the converter outputs its maximum current (1.25 pu), as shown in **Fig. 9**(a) and (b), respectively.

After the fault, the power generating capability of the WTs decreases to 0.68 pu. Thus, the active power control loop saturates, as shown in **Fig. 9**(c). The reactive powers increase and are shared among the WT converters, as shown in **Fig. 9**(d). The offshore frequency is well controlled near the rated value (i.e., 50 Hz), as shown in **Fig. 9**(e).

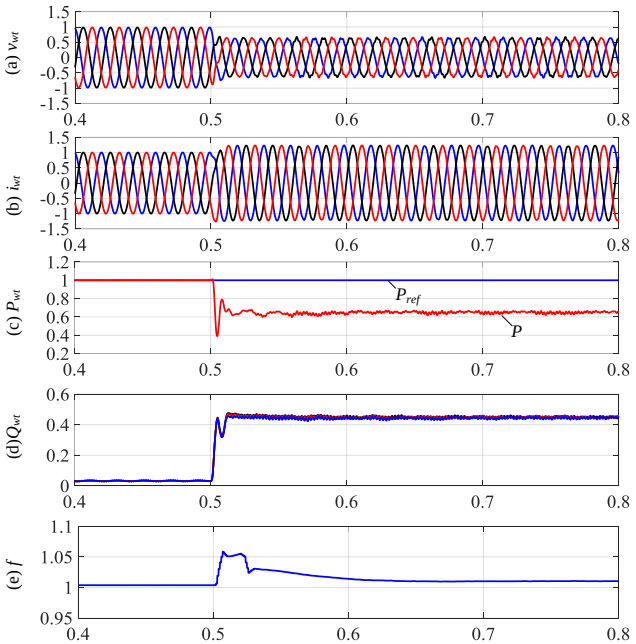

Fig. 9 Simulation results of WT converter during positive pole-to-ground DC cable fault in per-unit terms: (a) three-phase voltages, (b) three-phase currents, (c) active power, (d) reactive power, and (e) frequency.

5.3 DRU station internal faults

Before the fault, the system is operated at 0.6 pu active power, and an internal fault, F3 in **Fig. 1**, is initiated at DRU 1 at t=0.5 s, which leads to the effective short circuit of the DC terminal of DRU 1 (i.e., the DC voltage output from DRU 1 becomes zero).

When the fault occurs, the DC voltage of DRU 1 drops to zero while the DC voltages of the healthy DRUs, i.e., DRUs 2 and 3, remain near the rated value, as shown in **Fig. 10**(a). Thus, the DC voltage of the DRU-HVDC link

is reduced to two thirds of the rated DC voltage, as shown in **Fig. 10**(a). The onshore FB-MMC subsequently reduces the DC voltage to two thirds of the rated DC voltage. As the internal fault of DRU 1 leads to the short circuit of the AC side, large currents feed the fault from the WT converters through circuit breaker B_{D1}, as shown in **Fig. 10**(c). Thus, circuit breaker B_{D1} experiences overcurrent and is opened (at t=0.64 s for illustration) to isolate the faulty DRU 1.

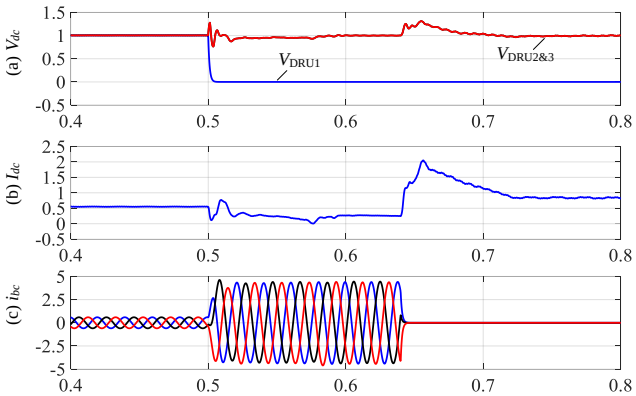

Fig. 10 Simulation results of offshore DRU station during internal DRU fault in per-unit terms: (a) DRU DC terminal voltages, (b) DC current, and (c) currents through breaker B_{D1}.

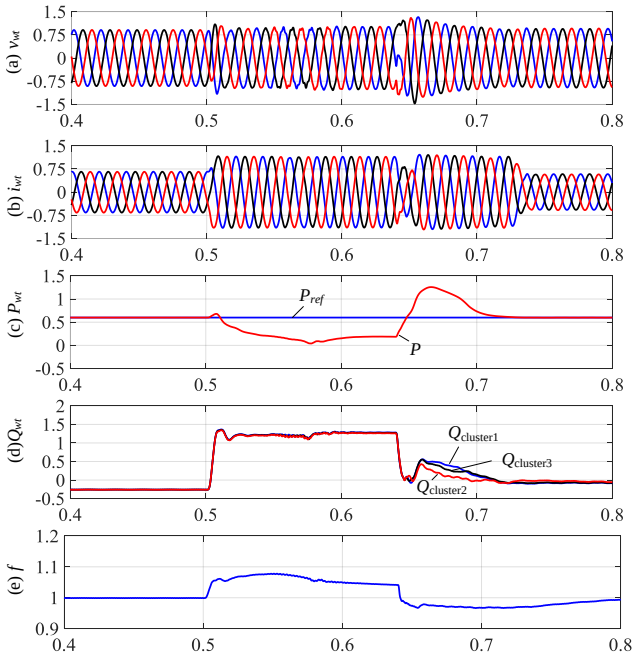

Fig. 11 Simulation results of WT converter during internal DRU fault in per-unit terms: (a) three-phase voltages, (b) three-phase currents, (c) active power, (d) reactive power, and (e) frequency.

Owing to the large fault current and leakage inductance of the DRU 1 transformer (0.18 pu), the offshore voltages do not drop significantly during the fault, as shown in **Fig. 11**(a). Thus, even during the fault, some generated power is still transmitted through the DRU-HVDC system to the onshore grid.

After the fault is isolated by circuit breaker B_{D1}, the system is operated with two DRUs, and the transmitted power autonomously resumes the pre-fault conditions (0.6 pu), as shown in **Fig. 11**(c) and **Fig. 12**(d). **Fig. 12**(c) shows that the onshore three-phase currents also restore to their pre-fault values. If the total power generated by the wind farm is larger than the maximum capability of the DRU-HVDC system after the disconnection of one DRU (reduced to approximately two thirds of the rated power), the active power control loop of the WTs will saturate and operate in voltage-limiting mode. The generated active power will then be automatically limited to two thirds of the rated power. This condition is not studied here owing to space limitations.

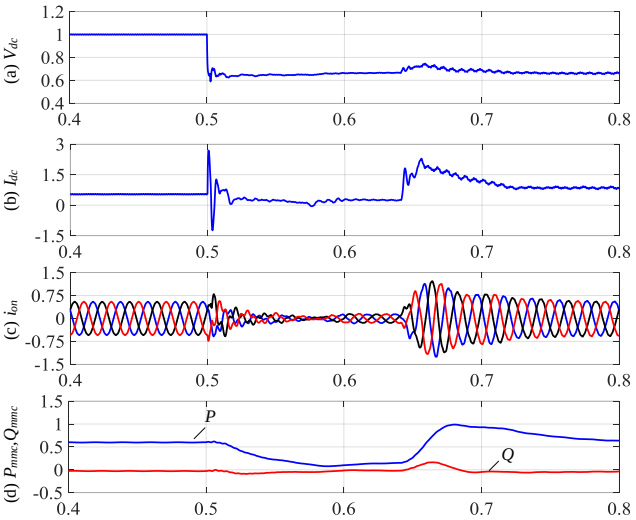

Fig. 12 Simulation results of onshore MMC during internal DRU fault in per-unit terms: (a) DC voltage, (b) DC current, (c) AC currents, and (d) active and reactive powers.

5.4 Offshore AC faults

To test the performance of the DRU-HVDC system during and after an offshore AC fault, a symmetrical solid AC fault, F4 in **Fig. 1**, is applied at the sting cable at t=0.5 s and isolated by breaker B_{BS1} at t=0.64 s.

After the fault, the offshore AC voltages collapse and the converter quickly increases the q-axis current (and thereby the reactive power) to provide fault currents and reduces the d-axis current to avoid overcurrent, as shown in **Fig. 13**(a), (d), and (b), respectively. The fault currents

provided by the WT converters (1.25 pu) feed into the fault through circuit breaker B_{S1}, which experiences a significant increase of fault currents, as shown in **Fig. 13**(f). By using overcurrent detection, breaker B_{S1} is opened at t=0.64 s (for illustration) to isolate the faulty string. The WT reactive power experiences slight oscillation during such a severe fault and gradually stabilizes with the regulation of the controller, as shown in **Fig. 13**(d).

The *d*-axis voltage control loop saturates during the fault, but it gradually restores the offshore voltage after the fault is isolated by B_{S1} at t=0.64 s, as shown in **Fig. 13**(a). The power transmitted by the WT and the DC current of the DRU-HVDC link rapidly restore, as shown in **Fig. 13**(c) and **Fig. 14**(b), respectively. During the entire process, the offshore frequency is well controlled near the rated value (i.e., 50 Hz), as shown in **Fig. 13**(e).

Fig. 13 and **Fig. 14** demonstrate that the WT converters automatically operate in a current-limiting mode during the string fault and quickly provide the required fault currents for fault detection. The system can automatically restore power transmission once the faulty branch is isolated.

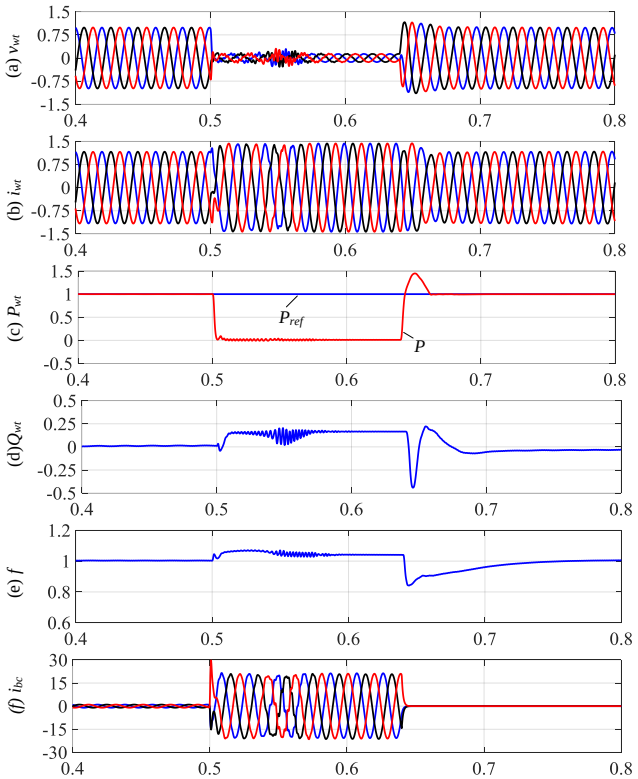

Fig. 13 Simulation results of WT converter during symmetrical offshore AC fault at string cables in per-unit terms: (a) three-phase voltages, (b) three-phase currents, (c) active power, (d) reactive power, (e) frequency, and (f) currents flowing through circuit breaker B_{S1}.

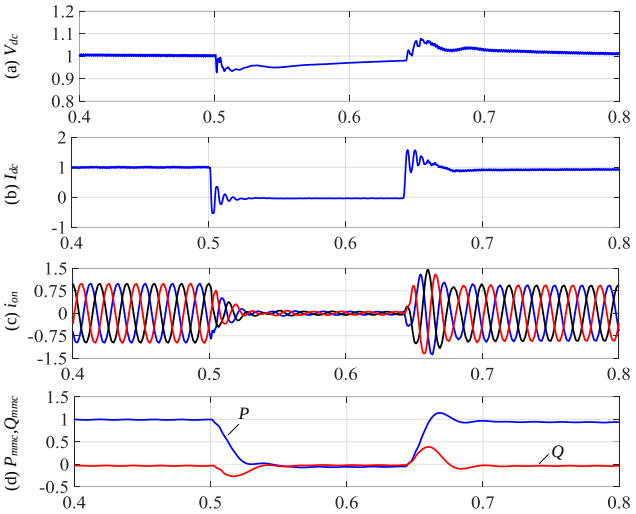

Fig. 14 Simulation results of onshore MMC during symmetrical offshore AC fault at string cables in per-unit terms: (a) DC voltage, (b) DC current, (c) AC currents, and (d) active and reactive powers.

6 Conclusion

The control and operation of OWFs connected using DRU-HVDC were investigated in this paper with particular consideration of faults including onshore and offshore AC grid faults, pole-to-pole and pole-to-ground DC faults, and internal DRU faults. The WT converters were controlled to operate autonomously in either current- or voltage-limiting mode during faults to ensure safe operation as well as provide adequate AC fault currents for offshore network protection. The studies demonstrate the robustness of the DRU-HVDC system against different faults and the automatic restoration of power transmission after fault isolation.

[1] S. M. Muyeen, R. Takahashi, and J. Tamura, "Operation and Control of HVDC-Connected Offshore Wind Farm," *IEEE Transactions on Sustainable Energy*, vol. 1, pp. 30-37, 2010.

[2] J. Liang, T. Jing, O. Gomis-Bellmunt, J. Ekanayake, and N. Jenkins, "Operation and Control of Multiterminal HVDC Transmission for Offshore Wind Farms," *IEEE Transactions on Power Delivery*, vol. 26, pp. 2596-2604, 2011.

[3] R. Blasco-Gimenez, S. A.-. Villalba, J. Rodríguez-D'Derlée, F. Morant, and S. Bernal-Perez, "Distributed Voltage and Frequency Control of Offshore Wind Farms Connected With a Diode-Based HVdc Link," *IEEE Transactions on Power Electronics*, vol. 25, pp. 3095-3105, 2010.

[4] S. Seman, R. Zurowski, and C. Taratoris, "Interconnection of advanced Type 4 WTGs with

Diode Rectifier based HVDC solution and weak AC grids," in *Proceedings of the 14th Wind Integration Workshop,Brussels, Belgium, 20th–22nd Oct.* , 2015.

[5] C. Prignitz, H. G. Eckel, S. Achenbach, F. Augsburger, and A. Schön, "FixReF: A control strategy for offshore wind farms with different wind turbine types and diode rectifier HVDC transmission," in *2016 IEEE 7th International Symposium on Power Electronics for Distributed Generation Systems (PEDG)*, 2016, pp. 1-7.

[6] T. H. Nguyen, D. C. Lee, and C. K. Kim, "A Series-Connected Topology of a Diode Rectifier and a Voltage-Source Converter for an HVDC Transmission System," *IEEE Trans. Power Electron.*, vol. 29, pp. 1579-1584, 2014.

[7] R. Blasco-Gimenez, S. Anó-Villalba, J. Rodriguez-D'Derlée, S. Bernal-Perez, and F. Morant, "Diode-Based HVdc Link for the Connection of Large Offshore Wind Farms," *IEEE Transactions on Energy Conversion*, vol. 26, pp. 615-626, 2011.

[8] S. Bernal-Perez, S. Ano-Villalba, R. Blasco-Gimenez, and J. Rodriguez-D'Derlee, "Efficiency and Fault Ride-Through Performance of a Diode-Rectifier- and VSC-Inverter-Based HVDC Link for Offshore Wind Farms," *IEEE Transactions on Industrial Electronics*, vol. 60, pp. 2401-2409, 2013.

[9] J. Guo, D. Jiang, Y. Zhou, P. Hu, Z. Lin, and Y. Liang, "Energy storable VSC-HVDC system based on modular multilevel converter," *International Journal of Electrical Power & Energy Systems*, vol. 78, pp. 269-276, 2016/06/01/ 2016.

[10] O. Kuhn, P. Menke, R. Zurowski, T. Christ, S. Seman, G. Giering, *et al.*, "2nd generation DC grid access for offshore wind farms: HVDC in an AC fashion," *CIGRE, Paris*, pp. 1-7, 2016.

[11] T. Kawaguchi, T. Sakazaki, T. Isobe, and R. Shimada, "Offshore-Wind-Farm Configuration Using Diode Rectifier With MERS in Current Link Topology," *IEEE Transactions on Industrial Electronics*, vol. 60, pp. 2930-2937, 2013.

[12] M. A. Cardiel-Alvarez, J. L. Rodriguez-Amenedo, S. Arnaltes, and M. Montilla-DJesus, "Modeling and Control of LCC Rectifiers for Offshore Wind Farms Connected by HVDC Links," *IEEE Transactions on Energy Conversion*, vol. PP, pp. 1-1, 2017.

[13] L. Yu, R. Li, and L. Xu, "Distributed PLL-based Control of Offshore Wind Turbine Connected with Diode-Rectifier based HVDC Systems," *IEEE Transactions on Power Delivery*, vol. PP, pp. 1-1, 2017.

[14] R. Li, L. Yu, and L. Xu, "Offshore AC Fault Protection of Diode Rectifier Unit Based HVDC System for Wind Energy Transmission," *IEEE Transactions on Industrial Electronics*, pp. 1-1, 2018.

[15] R. Zeng, L. Xu, L. Yao, and B. W. Williams, "Design and Operation of a Hybrid Modular Multilevel Converter," *IEEE Trans. Power Electron.*, vol. 30, pp. 1137-1146, 2015.

[16] R. Li, L. Xu, and D. Guo, "Accelerated switching function model of hybrid MMCs for HVDC system simulation," *IET Power Electronics*, 2017.

[17] L. Xu, L. Yao, and C. Sasse, "Grid Integration of Large DFIG-Based Wind Farms Using VSC Transmission," *IEEE Transactions on Power Systems*, vol. 22, pp. 976-984, 2007.

[18] W. Xiang, W. Lin, L. Xu, and J. Wen, "Enhanced Independent Pole Control of Hybrid MMC-HVDC System," *IEEE Transactions on Power Delivery*, vol. PP, pp. 1-1, 2017.